Journal of
Synchrotron
Radiation

ISSN 0909-0495

Received 13 December 2009
Accepted 24 April 2010

Quasi *in situ* Ni *K*-edge EXAFS investigation of the spent NiMo catalyst from ultra-deep hydrodesulfurization of gas oil in a commercial plant

Yusuke Hamabe,[a] Sungbong Jung,[a] Hikotaro Suzuki,[a] Naoto Koizumi[a]* and Muneyoshi Yamada[b]

[a]Department of Applied Chemistry, Graduate School of Engineering, Tohoku University, Aoba 6-6-07, Aramaki, Aoba-ku, Sendai 980-8579, Japan, and [b]Akita National College of Technology, 1-1 Iijima-Bunkyo-cho, Akita 011-8511, Japan. E-mail: koizumi@erec.che.tohoku.ac.jp

Ni species on the spent NiMo catalyst from ultra-deep hydrodesulfurization of gas oil in a commercial plant were studied by Ni *K*-edge EXAFS and TEM measurement without contact of the catalysts with air. The Ni–Mo coordination shell related to the Ni–Mo–S phase was observed in the spent catalyst by quasi *in situ* Ni *K*-edge EXAFS measurement with a newly constructed high-pressure chamber. The coordination number of this shell was almost identical to that obtained by *in situ* Ni *K*-edge EXAFS measurement of the fresh catalyst sulfided at 1.1 MPa. On the other hand, large agglomerates of Ni_3S_2 were observed only in the spent catalyst by quasi *in situ* TEM/EDX measurement. MoS_2-like slabs were sintered slightly on the spent catalyst, where they were destacked to form monolayer slabs. These results suggest that the Ni–Mo–S phase is preserved on the spent catalyst and Ni_3S_2 agglomerates are formed by sintering of Ni_3S_2 species originally present on the fresh catalyst.

Keywords: NiMo catalyst; Ni–Mo–S phase; ultra-deep hydrodesulfurization; catalyst deactivation; quasi *in situ* Ni *K*-edge EXAFS.

1. Introduction

Ultra-deep hydrodesulfurization (HDS) of gas oil is an important process for producing ultra-low-sulfur diesel fuel (<10 mass p.p.m.-S). It was recently found that CoMo and NiMo catalysts were severely deactivated during ultra-deep HDS of gas oil at the beginning of time on stream (Fujikawa *et al.*, 2006; NEDO, 2002). To prevent deactivation of the catalysts, it is important to clarify the deactivation mechanism of these catalysts. However, only a few papers have been published that investigate the deactivation mechanism of the catalyst for ultra-deep HDS of gas oil (Koizumi *et al.*, 2005*a*,*b*, 2006; Eijsbouts *et al.*, 2005, 2007; de la Rosa *et al.*, 2004; Guichard *et al.*, 2008, 2009).

On the other hand, extensive studies have been made to clarify the deactivation mechanism of the catalyst for HDS of heavy oil (Christensen *et al.*, 1994; Iijima *et al.*, 1997; Gualda & Kasztelan, 1994; Furimsky & Massoth, 1999; Yamazaki *et al.*, 1999; Fujii *et al.*, 2000; Idei *et al.*, 2002*a*,*b*, 2003; Ternan *et al.*, 1979; Egiebor *et al.*, 1989; Díez *et al.*, 1990, 1992; de Jong *et al.*, 1991, 1994; Hadjiloizou *et al.*, 1992; Zeuthen *et al.*, 1994, 1995; Marafi & Stanislaus, 1997; Koide *et al.*, 1999; Seki & Yoshimoto, 2001*a*,*b*,*c*,*d*; Kumata *et al.*, 2001; Callejas *et al.*, 2001; Higashi *et al.*, 2002; Amemiya *et al.*, 2003; Sahoo *et al.*, 2004; Hauser *et al.*, 2005; Eijsbouts & Inoue, 1994). Based on these studies, it has been suggested that catalyst deactivation is caused by (i) deposition of V and/or Ni sulfides originated from metalloporphyrin compounds in heavy oil (Christensen *et al.*, 1994; Iijima *et al.*, 1997; Gualda & Kasztelan, 1994; Furimsky & Massoth, 1999; Yamazaki *et al.*, 1999; Fujii *et al.*, 2000; Idei *et al.*, 2002*a*,*b*, 2003), (ii) deposition of carbonaceous compounds (Gualda & Kasztelan, 1994; Furimsky & Massoth, 1999; Yamazaki *et al.*, 1999; Fujii *et al.*, 2000; Idei *et al.*, 2002*a*,*b*, 2003; Ternan *et al.*, 1979; Egiebor *et al.*, 1989; Díez *et al.*, 1990, 1992; de Jong *et al.*, 1991, 1994; Hadjiloizou *et al.*, 1992; Zeuthen *et al.*, 1994, 1995; Marafi & Stanislaus, 1997; Koide *et al.*, 1999; Seki & Yoshimoto, 2001*a*,*b*,*c*,*d*; Kumata *et al.*, 2001; Callejas *et al.*, 2001; Higashi *et al.*, 2002; Amemiya *et al.*, 2003; Sahoo *et al.*, 2004; Hauser *et al.*, 2005), and (iii) solid-state transformation of sulfide phases such as sintering and/or decomposition of HDS active phase(s) (Gualda & Kasztelan, 1994; Eijsbouts & Inoue, 1994). During ultra-deep HDS of gas oil, deposition of V and/or Ni sulfides is negligible because gas oil never contains metalloporphyrin compounds. The authors recently investigated the nature of carbonaceous compounds deposited on spent $NiMoP/Al_2O_3$ catalysts from ultra-deep HDS of gas oil. Laser Raman measurement revealed that carbonaceous compounds with amorphous structure were deposited on the spent catalysts sampled from the inlet region of the catalyst bed, whereas carbonaceous compounds on the

spent catalysts sampled from the outlet region of the catalyst bed had graphite-like structure (Koizumi *et al.*, 2005*a*,*b*). The molecular weight of the carbonaceous compound with graphite-like structure was estimated at approximately 1.5 kDa by laser desorption/ionization TOFMS measurement (Koizumi *et al.*, 2006). HDS activity of the spent catalysts linearly decreased with increasing the amount of the carbonaceous compound with graphite-like structure. Based on these results, deposition of this type of carbonaceous compound was suggested to be linked with catalyst deactivation.

In order to investigate the deactivation mechanism of the NiMo catalyst from a different point of view, an attempt has been made to clarify the structural change of the HDS active phase, *i.e.* the Ni–Mo–S phase, in this work. Ni *K*-edge EXAFS spectroscopy is a powerful tool for investigating the coordination structure of Ni species without long-range order. However, Ni *K*-edge EXAFS measurement of conventional Al_2O_3-supported NiMo catalysts were quite limited because of difficulties in obtaining EXAFS spectra with appropriate signal-to-noise ratio. So far, *ex situ* transmission electron microscope (TEM), TEM/EDX (energy-dispersive X-ray) and X-ray diffraction (XRD) measurements have been performed to investigate the surface structure of spent CoMo (Eijsbouts *et al.*, 2007) and NiMo (Eijsbouts *et al.*, 2005) catalysts from ultra-deep HDS of gas oil. Ni *K*-edge EXAFS of the spent NiMo catalyst from ultra-deep HDS of gas oil has not been reported yet.

Furthermore, the surface structure of the spent catalyst should be compared with that of the fresh catalyst sulfided at high pressure to clarify the deactivation mechanism, because the catalyst is exposed to a high-pressure sulfiding atmosphere under ultra-deep HDS conditions. In our previous work (Koizumi *et al.*, 2010), a high-pressure EXAFS chamber equipped with Cu-free polybenzimidazol (PBI) windows was newly constructed. *In situ* Ni and Mo *K*-edge EXAFS measurements with this high-pressure chamber successfully probed the Ni–Mo and Mo–Ni coordination shells related to the Ni–Mo–S phase in $NiMo/Al_2O_3$ catalysts sulfided at high pressure (613 K, 1.1 MPa). It was also revealed that Ni *K*-edge EXAFS spectra of NiMo/graphite catalysts reported by Louwers & Prins (1992) were contaminated with a small amount of Cu impurity contained in beryllium windows used for their EXAFS chamber. In other words, the newly constructed high-pressure chamber is suitable for investigating the deactivation mechanism of the NiMo catalyst. Another important point is the use of quasi *in situ* characterization techniques. Because nanometre-sized sulfide clusters have higher reactivity towards air exposure, the spent catalyst will suffer from severe oxidation once the spent catalyst comes into contact with air. This may lead to misleading conclusions concerning the deactivation mechanism.

In the present study this high-pressure chamber was used for quasi *in situ* Ni *K*-edge EXAFS measurement of the deactivated catalyst in order to obtain a deeper understanding of the deactivation mechanism of the NiMo catalyst under ultra-deep HDS conditions. *Ex situ* XRD and quasi *in situ* TEM/EDX measurements were also performed to investigate the morphological change of Ni and Mo species during ultra-deep HDS of gas oil.

2. Experimental

2.1. Spent catalyst

A $NiMoP/Al_2O_3$ catalyst (oxide precursor) was prepared and supplied by a petroleum company of Japan. Detailed preparation procedures were not disclosed by the petroleum company. The BET surface area of this catalyst was 124 m^2 g-cat^{-1}. On an Al_2O_3 weight basis, this catalyst had 245 m^2 g-$Al_2O_3{}^{-1}$ of the surface area comparable with the value of its Al_2O_3 support. An XRD pattern of this catalyst showed only broad diffraction peaks related to the γ-Al_2O_3 phase.

The $NiMoP/Al_2O_3$ catalyst was loaded and subjected to ultra-deep HDS of straight run gas oil (SRGO) in a commercial HDS unit after sulfiding pretreatment in a liquid phase. The sulfur content of SRGO was approximately 10^4 mass p.p.m.-S. The reaction temperature was adjusted so that the total sulfur content of the product oil was maintained below 10–50 mass p.p.m.-S. H_2 partial pressure and space velocity were 5.0 MPa and approximately 1 h^{-1}, respectively. After ultra-deep HDS of gas oil for two years, the spent $NiMoP/Al_2O_3$ catalysts were sampled and stored in a bottle filled with kerosene in order to avoid contact with air.

To evaluate the HDS activity of these spent catalysts, HDS of SRGO was performed in a bench scale plant with these spent catalysts (Koizumi *et al.*, 2006). The HDS activity of the spent catalysts was a function of the sampling position from the catalyst bed. The spent catalysts sampled from the inlet region of the catalyst bed had 70% of HDS activity of the fresh catalyst even after ultra-deep HDS of gas oil for two years, whereas severe deactivation was observed for the spent catalysts sampled from the outlet region of the catalyst bed (approximately 20% of HDS activity of the fresh catalyst). It was revealed that HDS activity of the spent catalysts linearly decreased with the amount of carbonaceous compound with graphite-like structure. In this paper, quasi *in situ* characterization data of the spent catalyst sampled from the outlet region of the catalyst bed are discussed to obtain a clear insight into the deactivation mechanism.

2.2. Pretreatment of the spent catalyst

Because the spent catalyst was submerged under kerosene during storage, the kerosene had to be removed before catalyst characterization. This was carried out in a glove box filled with N_2 (O_2 content = 10–20 vol. p.p.m.) to avoid contact with air. Firstly, the spent catalyst was rinsed with toluene followed by drying at ambient temperature for 0.5 h. Then the spent catalysts were ground into fine powder in a mortar and pestle. Some of powdered catalysts were formed into a disc (diameter 14 mm, $\Delta\mu t$ = 0.7–1.0) for quasi *in situ* Ni *K*-edge EXAFS measurement. This disc was then set in the high-pressure EXAFS chamber mentioned below. For quasi *in situ* TEM/EDX measurement, powdered catalysts were suspended in

alcohol solution. This suspension was stored in a bottle filled with N_2.

2.3. *Ex situ* XRD measurement

XRD patterns of the spent and fresh catalysts were measured on a R_{int} X-ray diffractometer (Rigaku). Cu $K\alpha$ radiation (λ = 1.54056 Å) was used as an X-ray source with an X-ray tube operating at 40 kV and 200 mA. The $NiMoP/Al_2O_3$ catalyst (oxide precursor) was subjected to sulfiding pretreatment at 673 K and 4.1 MPa in a 5% H_2S/H_2 (>99.99995%) stream using a fixed-bed reactor before XRD measurement. Hereafter, the catalyst sulfided in the gas phase is denoted as fresh-g. After presulfiding treatment, the catalyst was passivated in a stream of 1% O_2/He at ambient temperature. Diffraction intensities were recorded at a scan speed of $0.02^\circ\ s^{-1}$. The observed diffraction peaks were assigned by referring to JCPDS (Joint Committee on Powder Diffraction Standards) data.

The lengths (D_{hkl}) of the MoS_2 slabs along the stacking and basal directions were calculated using the Debye–Scherrer equation,

$$D_{hkl} = \frac{k_{hkl}\lambda}{\beta_{hkl}\cos\theta}, \quad (1)$$

where λ is the wavelength of the X-rays (λ = 1.54056 Å) and β_{hkl} (or FWHM) is the angular line width. In the case of MoS_2, the shape factor k_{002} was equal to 0.76 and k_{110} was 1.42–1.56 (Liang *et al.*, 1986). The average stacking number of the MoS_2 slab was calculated using $\overline{n} = D_{002}/6.17$, the value of 6.17 Å corresponding to the interlayer spacing in the 2H-MoS_2 structure.

2.4. Quasi *in situ* TEM/EDX measurement

The morphology of Ni and Mo species on the spent catalyst was investigated by quasi *in situ* TEM/EDX measurement. For this measurement a few droplets of alcohol suspension prepared in a glove box were dropped onto a carbon-coated Cu grid followed by drying at ambient temperature. The sample was transferred into a vacuum chamber and subjected to TEM/EDX measurement using an HF-2000 TEM (Hitachi) with 200 kV accelerate voltage. Typically 28 micrographs were taken for each sample. 349–644 MoS_2 slabs were analyzed to calculate the distribution of the slab length and stacking number. The average MoS_2 slab length ($\overline{L}$) and stacking number ($\overline{N}$) were calculated using the following equations,

$$\log \overline{L} = \frac{\sum n_i \log L_i}{\sum n_i}, \quad (2)$$

$$\overline{N} = \frac{\sum n_i N_i}{\sum n_i}, \quad (3)$$

where n_i is the number of the MoS_2 slab having L_i, N_i characteristics. Elemental mappings were obtained by EDX measurement (Noran Instruments).

For quasi *in situ* TEM/EDX measurement of the fresh catalyst, sulfiding pretreatment was performed in a 5% H_2S/H_2 stream at 673 K and 4.1 MPa using the stainless steel fixed-bed reactor (diameter 4 mm). After sulfiding pretreatment, the catalyst was cooled down to ambient temperature in the 5% H_2S/H_2 (>99.99995%) stream (fresh-g). The reactor was then flushed with an H_2 (>99.999%) stream to remove residual H_2S, and transferred into the glove box. For comparison, liquid-phase sulfiding pretreatment was also conducted. The catalyst was soaked with 4 mass% dimethyl disulfide-spiked model gas oil (1 mass% dibenzothiophene/39.6 mass% 1-methylnaphthalene/59.4 mass% *n*-hexadecane) in the H_2 stream at 4.1 MPa using the fixed-bed reactor. The temperature was kept at 373 K for 3 h, 523 K for 8 h, and then 593 K for 5 h, while the catalyst was heated at a rate of $1\ K\ min^{-1}$. After sulfiding pretreatment, the catalyst was cooled down to room temperature. The catalyst was then rinsed with toluene in an H_2 stream at 4.1 MPa (fresh-liq). The following procedures were the same as those employed for the spent catalyst.

2.5. Quasi *in situ* EXAFS measurement

EXAFS measurement was conducted at the synchrotron radiation facilities in Japan (PF and SPring-8). Ni *K*-edge EXAFS spectra were measured at BL9C (PF) and BL14B2 (SPring-8) with ring energies of 2.5 and 8 GeV, respectively. The X-rays passed through a Si(111) double-crystal monochromator and focused onto the sample. The EXAFS data were collected in transmission mode using I_0 and I ionization chambers filled with 100% N_2 and 15% Ar/N_2, respectively.

The high-pressure EXAFS chamber was used for quasi *in situ* and *in situ* measurement. This chamber was made of SUS316 stainless steel and designed for transmission EXAFS measurement. Details of this chamber were reported in our previous paper (Koizumi *et al.*, 2010). The high-pressure chamber was connected with flow apparatus equipped with mass flow controllers (Brooks Instruments, 5850E) and back-pressure regulators (TESCOM). EXAFS spectra were measured at ambient temperature under high-pressure H_2 atmosphere (>99.9995%, approximately 1.0 MPa). *In situ* Ni *K*-edge EXAFS of the fresh catalyst was measured under flowing H_2 at ambient temperature after sulfiding pretreatment using a 5% H_2S/H_2 (>99.99995%) stream at 613 K and 1.1 MPa (fresh-g). Detailed procedures for *in situ* measurement can be found in our previous paper (Koizumi *et al.*, 2010).

2.6. EXAFS analysis

The observed EXAFS spectra were analyzed in a conventional manner including background subtraction and normalization followed by Fourier filtering using a Rigaku XAFS data analysis system (REX2000). Contributions from coordination shells in the Fourier-transformed $k^3\chi(k)$ were then inverse Fourier transformed using a Hanning-type window function into k space. Structural parameters of each coordination shell were determined by a non-linear least-square fitting in k space. The backscattering amplitude and phase shift of the Ni–O, Ni–S, Ni–Ni and Ni–Mo coordination shells were calculated using *FEFF8.4* code (Ankudinov *et al.*,

1998) using the NiO (Ni–O) (Rooksby, 1948), NiS_2 (Ni–S) (Nowack *et al.*, 1991), Ni (Ni–Ni) (Swanson & Tatge, 1953) and $Ni_{2.5}Mo_6S_8$ (Ni–Mo) (Chang *et al.*, 1987) structures, respectively. In the non-linear least-square fitting of the spectrum of the spent catalyst, the inner potential and Debye–Waller factor of each coordination shell were fixed at the values obtained from the polycrystalline NiO, Ni_3S_2 (Aldrich, purity >99.7%) and Ni foil. This was necessary to make the number of parameters comparable with the number of independent parameters (N_{idp}) (Stern, 1993) defined as follows,

$$N_{idp} = (2\Delta k \Delta R/\pi) + 2. \quad (4)$$

Curve-fitting analysis was then conducted, where reducing factors (S_0^2) (Roy & Gurman, 1999) for the Ni–O, Ni–S and Ni–Ni coordination shells were fixed at 0.47, 0.73 and 0.85. These values were obtained by fitting the Ni–O, Ni–S and Ni–Ni contributions in the Ni *K*-edge EXAFS of the polycrystalline NiO, Ni_3S_2 and Ni foil. The quality of the fitting was calculated using the *R*-factor (R_f) defined by the following equation,

$$R_f\ (\%) = \left\{ \frac{\sum_i \left[k^3\chi_i^{obs}(k) - k^3\chi_i^{cal}(k)\right]^2}{\sum_i \left[k^3\chi_i^{obs}(k)\right]^2} \right\} \times 100. \quad (5)$$

The distribution of Ni species in the fresh and spent catalysts was evaluated by pattern-fitting analysis of *in situ* and quasi *in situ* Ni *K*-edge XANES spectra. The quality of the fitting was evaluated by the following equation,

$$R_f\ (\%) = \left[\sum (I_{obs} - I_{cal})^2 / \sum (I_{obs})^2\right] \times 100. \quad (6)$$

3. Results

3.1. Crystalline phases on the spent catalyst

The spent catalyst was subjected to *ex situ* XRD measurement to investigate crystalline Ni and Mo phases formed in the spent catalyst. Fig. 1 compares *ex situ* XRD patterns of the spent and fresh-g catalysts. The fresh-g catalyst was sulfided at 673 K and 4.1 MPa followed by passivation before XRD measurement. In the diffraction pattern of the fresh-g catalyst, broad diffraction peaks were observed at 2θ = 14, 33, 37, 45, 59 and 67°. The peaks at 2θ = 14, 33, 37 and 59° were assigned to the 2H-MoS_2 phase, whereas the remaining peaks were assigned to the γ-Al_2O_3 phase. No diffraction peaks were observed related to other Ni and Mo phases in this pattern. On the other hand, additional sharp peaks were observed at 2θ = 22, 31, 38, 44, 50 and 55° in the diffraction pattern of the spent catalyst. All these 2θ values coincided well with those of the diffraction peaks of the Ni_3S_2 phase, showing that the crystalline Ni_3S_2 species is formed in the spent catalyst. The crystalline size of the Ni_3S_2 phase was estimated at approximately 25 nm by the Debye–Scherrer equation using the full width at half-maximum of the Ni_3S_2 (101) peak (2θ = 22°). The lateral size [(110) direction] of the 2H-MoS_2 phase was also estimated by the Debye–Scherrer equation (Table 1). The lateral size of the MoS_2 phase in the spent catalyst was slightly larger than those in the fresh-g catalyst, showing that the MoS_2 species was slightly sintered during ultra-deep HDS of gas oil. However, this sintering was not so serious; the number of edge and corner sites of the MoS_2-like slabs was still 90% of the total Ni atoms in the spent catalyst. On the other hand, the stacking degree of the 2H-MoS_2 phase in the fresh-g and spent catalysts was identical (Table 1).

Table 1
Length and stacking number of the MoS_2 slabs over the fresh and spent catalysts.

	Length (nm)			Stacking number		
	Fresh-g	Fresh-liq	Spent	Fresh-g	Fresh-liq	Spent
Ex situ XRD	4.0	–	4.9	2.4	–	2.5
Quasi *in situ* TEM	4.3	3.7	4.7	2.7	2.2	2.0

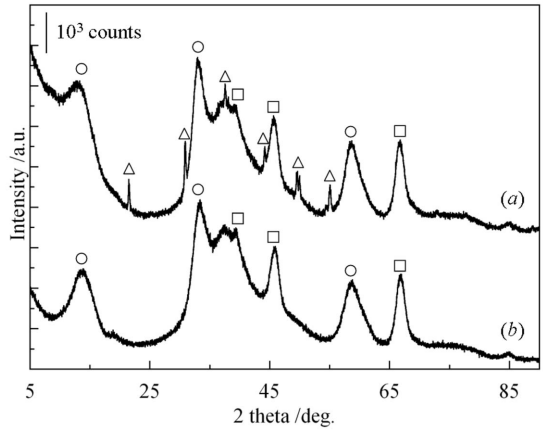

Figure 1
Ex situ XRD patterns of the spent (*a*) and fresh-g (*b*) catalysts. The fresh-g catalyst was sulfided in a 5% H_2S/H_2 stream at 673 K and 4.1 MPa. Circles: 2H-MoS_2; squares: γ-Al_2O_3; triangles: Ni_3S_2.

3.2. Morphology of Ni and Mo species on the spent catalyst

XRD measurement provided structural information related to the crystalline phases in the spent catalyst. To investigate the morphology of the Ni and Mo species in microscopic order, the spent and fresh catalysts were subjected to quasi *in situ* TEM/EDX measurement.

3.2.1. Ni species. The distribution of Ni species over the spent catalyst was investigated first by quasi *in situ* TEM/EDX measurement. Fig. 2(*a*) shows EDX mappings of S, Ni and Mo species in the spent catalyst, in comparison with those in the fresh-g catalyst sulfided at 673 K and 4.1 MPa (Fig. 2*b*). The EDX mappings of S, Ni and Mo species in the fresh-g catalyst showed uniform distribution of these species. In particular, the distribution of Ni and Mo species coincided well with each other, showing that Ni and Mo species were well mixed in submicrometre order. A total of ten EDX mappings were taken for the fresh-g catalyst. No agglomerates of Ni and Mo species were observed even in high-magnification EDX mappings (not shown here). Similar to the fresh-g catalyst, the EDX mappings for the spent catalyst showed uniform distribution of S and Mo species. However, a marked difference was seen in the EDX mapping of Ni species, where Ni species

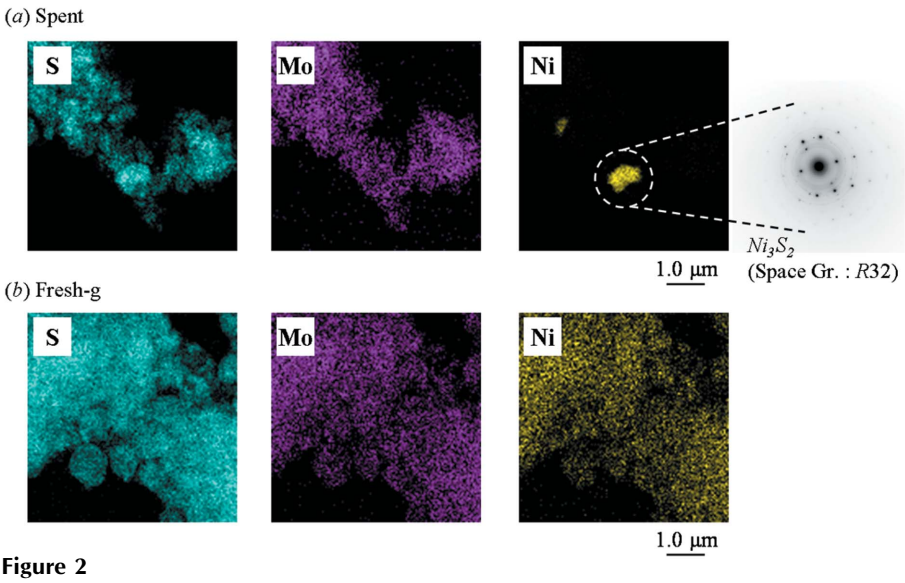

Figure 2
TEM/EDX mapping for S (blue), Mo (purple) and Ni (yellow) species over spent (*a*) and fresh-g (*b*) catalysts. An electron diffraction pattern is also included in (*a*).

formed ~300 nm-sized agglomerates. Similar agglomerates were observed in a total of four out of ten EDX mappings. Electron diffraction analysis showed that this agglomerate had Ni_3S_2 structure [see inset in Fig. 2(*a*)]. On the other hand, the crystalline size of Ni_3S_2 species was estimated at approximately 25 nm by the Debye–Scherrer equation. Thus, it was suggested that relatively small (below 25 nm) Ni_3S_2 crystallites were accumulated to form the large agglomerate. From simple estimation, the local density of Ni in this agglomerate was 25 times larger than that of Ni in the fresh-g catalyst. Both *ex situ* XRD and quasi *in situ* TEM/EDX measurements showed that the Ni species was significantly sintered during ultra-deep HDS of gas oil to form large N_3S_2 agglomerates.

Eijsbouts *et al.* (2005) recently reported that Ni_3S_2 agglomerates (5–50 nm size) were observed by *ex situ* TEM/EDX measurement of the spent NiMo catalyst from ultra-deep HDS of light gas oil, whereas MoS_2 dispersion calculated from TEM images was still high. Therefore, they suggested that Ni atoms were segregated from the Ni–Mo–S phases during ultra-deep HDS of gas oil. Similarly, Co sulfide agglomerates were observed by *ex situ* TEM/EDX measurement of the spent CoMo catalysts from ultra-deep HDS of gas oil in commercial plants for two years (Eijsbouts *et al.*, 2007). The Ni_3S_2 agglomerates observed in this work had much larger sizes compared with those reported by the previous studies.

3.2.2. Mo species. Figs. 3(*a*) and 3(*b*) show typical quasi *in situ* TEM micrographs of the fresh-g and spent catalysts. 28 micrographs were taken for each catalyst. Multilayered 5–10 nm-sized MoS_2-like slabs were uniformly distributed in these micrographs. 638–644 MoS_2-like slabs were analyzed for each catalyst to calculate the distribution of their slab length (Fig. 4*a*) and stacking number (Fig. 4*b*). These figures also include distribution of the length and stacking number of the MoS_2-like slabs in the fresh-liq catalyst. The average slab length and stacking number are tabulated in Table 1. Compared with the fresh-g and fresh-liq catalysts, the spent catalyst had a larger fraction of the slab length above 4 nm. The average slab length of the MoS_2-like slabs in these catalysts decreased in the following order: spent > fresh-g > fresh-liq (Table 1). The lengths of the MoS_2-like slabs in the fresh-g and spent catalyst were almost identical to the value calculated by the Debye–Scherrer equation.

A clearer difference was seen in the distribution of the stacking degree of the MoS_2-like slabs (Fig. 4*b*). The major

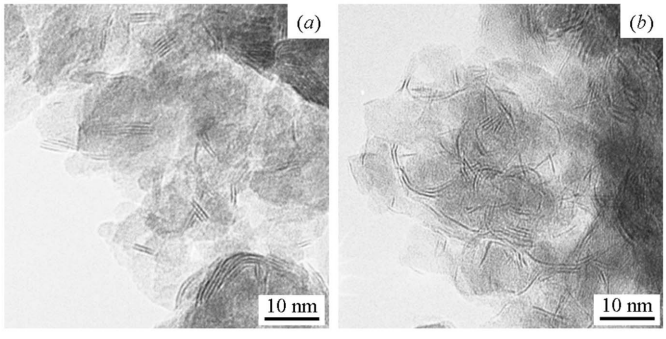

Figure 3
Quasi *in situ* TEM images of fresh-g (*a*) and spent (*b*) catalysts. The fresh-g catalyst was sulfided in a 5% H_2S/H_2 stream at 673 K and 4.1 MPa.

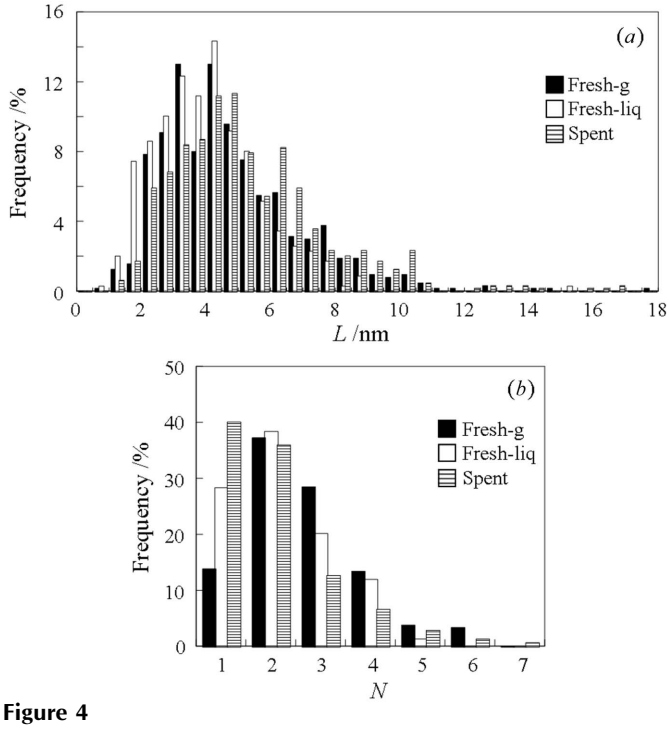

Figure 4
Distribution of MoS_2 slab length (*a*) and stacking number (*b*) for fresh-g, fresh-liq and spent catalysts.

fractions were present as two- or three-layered slabs in the fresh-g and fresh-liq catalysts (approximately 60–70%). The fraction of the monolayer slabs was only 10–30%. Compared with these fresh catalysts, the spent catalyst had a lower fraction of three-layered slabs, whereas the fraction of the monolayer slab reached 40%. The average stacking number of the slabs in the spent catalyst was the lowest as well. It is also seen from Table 1 that quasi *in situ* TEM measurement provided the lower average stacking number of the slabs in the spent catalyst compared with the value calculated by the Debye–Scherrer equation. This is probably because the monolayer MoS_2-like slabs were not observed by the XRD measurement. Quasi *in situ* TEM measurement provided 2.7 of the average stacking number of the slabs in the spent catalyst when the monolayer MoS_2-like slabs were excluded from the calculation, which was almost identical to the value calculated by the Debye–Scherrer equation. From these results it was suggested that the MoS_2-like slabs (or the Ni–Mo–S phase) were slightly sintered during ultra-deep HDS of gas oil, whereas they were destacked to form the monolayer slab. The monolayer slab accounted for 40% of the total MoS_2-like slabs (or the Ni–Mo–S phases) in the spent catalyst.

3.3. Coordination structure of Ni in the spent catalyst

To clarify the origin of Ni sulfide species in the spent catalyst, the coordination structure of Ni species in the spent catalyst was further investigated by quasi *in situ* Ni *K*-edge EXAFS, and compared with that obtained by *in situ* measurement. For easy understanding of the EXAFS results, *in situ* Ni *K*-edge EXAFS of the fresh-g catalyst is presented first.

3.3.1. Fresh-g catalyst. Fig. 5(*a*) displays a Ni *K*-edge $k^3\chi(k)$ spectrum of the fresh-g catalyst measured at ambient temperature after sulfiding pretreatment at 613 K and 1.1 MPa. Use of the high-pressure chamber equipped with PBI windows provided EXAFS oscillation with higher signal-to-noise ratio. EXAFS oscillation was clearly distinguishable from the noise even in the higher k range. The maximum k value for the Fourier transform (FT) reached around 148 nm^{-1} as indicated by k_{max} in the figure, whereas the FT range was limited to a maximum of 110 nm^{-1} in the previous study using the NiMo/graphite catalyst sulfided at atmospheric pressure (Louwers & Prins, 1992). A higher k_{max} value was essential for clear observation of the Ni–Mo coordination shell related to the Ni–Mo–S phase (Koizumi *et al.*, 2010). This $k^3\chi(k)$ spectrum was then Fourier transformed in the FT range defined by k_{min} and k_{max} shown in Fig. 5(*a*). Thus the obtained Ni *K*-edge FT-EXAFS spectrum is shown in Fig. 5(*c*). In this spectrum the main peak was observed at around 0.18 nm with a weak peak at around 0.24 nm (not phase-shift corrected).

In our previous work (Koizumi *et al.*, 2010) the effect of sulfiding temperature and Ni to Mo molar ratio on the coordination structure of Ni and Mo species on $NiMo/Al_2O_3$ catalysts was systematically investigated by *in situ* Ni and Mo *K*-edge EXAFS measurement. The catalysts were prepared by the conventional stepwise impregnation method followed by drying and calcination, and had normal Mo loading (15 mass% as MoO_3). *In situ* Ni and Mo *K*-edge EXAFS successfully probed the Ni–Mo and Mo–Ni coordination shells related to the Ni–Mo–S phase in the $NiMo/Al_2O_3$ catalyst sulfided at high pressure (613 K, 1.1 MPa). The Ni–Mo coordination shell of the Ni–Mo–S phase showed a weak peak at around 0.24 nm (not phase-shift corrected) in the Ni *K*-edge FT-EXAFS spectra. The Ni–Mo–S phase was only the Ni species observed in the spectra when the Ni to Mo molar ratio was low (0.2). At ratios higher than 0.4 the formation of other Ni species, NiO_x (NiO and/or $NiAl_2O_4$-like species) and Ni_3S_2, was observed in the catalysts.

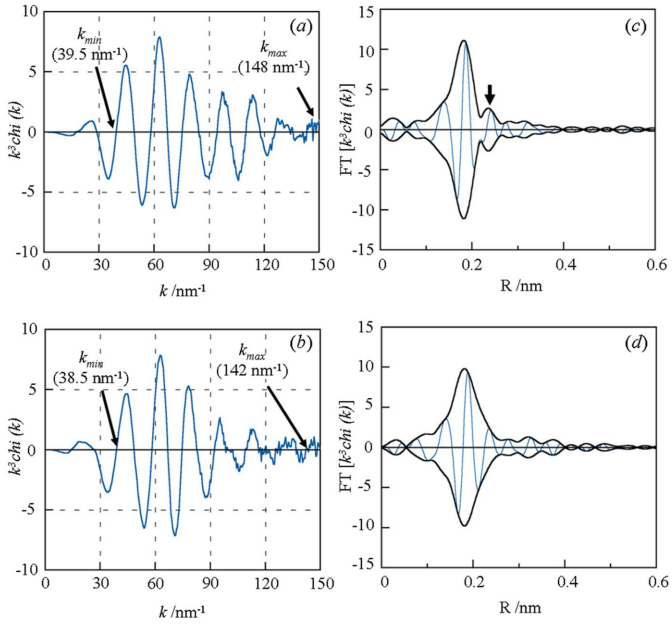

Figure 5
Ni *K*-edge $k^3\chi(k)$ of fresh-g (*a*) and spent (*b*) catalysts and their Fourier transforms in the k range indicated by k_{min} and k_{max} (*c*), (*d*). (*a*), (*c*) X-ray absorption spectrum measured at ambient temperature after sulfiding pretreatment at 613 K and 1.1 MPa using the high-pressure chamber. (*b*), (*d*) X-ray absorption spectrum measured under high-pressure H_2 atmosphere (~1.0 MPa) after rinsing with toluene in a glove box filled with N_2.

In the Ni *K*-edge FT-EXAFS spectrum of the fresh-g catalyst, a weak peak was observed at around 0.24 nm (not phase-shift corrected) in the Ni *K*-edge FT-EXAFS spectrum (Fig. 5*c*) as indicated by the arrow, suggesting the formation of the Ni–Mo coordination shell related to the Ni–Mo–S phase. Curve-fitting analysis of this spectrum was firstly performed using Ni–O (NiO_x species), Ni–S (Ni_3S_2 species + Ni–Mo–S phase), Ni–Ni (Ni_3S_2 species) and Ni–Mo (Ni–Mo–S phase) coordination shells based on EXAFS analysis of our home-made catalysts. However, the EXAFS spectrum of the fresh catalyst could also be fitted well by using only the Ni–S, Ni–Ni and Ni–Mo coordination shells. The Ni–O coordination shell was not necessarily required to obtain a satisfied fitting quality ($R_f < 1\%$). Fitting results obtained using the Ni–S, Ni–Ni and Ni–Mo coordination shells are shown in Figs. 6(*a*) and 6(*b*). Good fitting was obtained between experimental and calculated spectra in both k and R space. The R_f value defined by

Table 2
Fitting results for FT of Ni *K*-edge $k^3\chi(k)$ of fresh and spent catalysts.

CN: coordination number. *R*: distance. E_0: inner potential. σ^2: Debye–Waller factor. R_f: *R*-factor. EXAFS measurements were conducted at ambient temperature after sulfiding pretreatment.

Catalyst	Scattering pair	CN	*R* (nm)	E_0 (eV)	σ^2 (10^{-5} nm^2)	R_f (%)
Fresh-g	Ni–S	4.8 ± 0.3	0.220 ± 0.001	−5.821	5.04	0.34
	Ni–Ni	0.3 ± 0.2	0.252 ± 0.004	2.736	1.44	
	Ni–Mo	0.6 ± 0.2	0.277 ± 0.002	2.194	2.81	
Spent†	Ni–O	1.3 ± 0.6	0.204 ± 0.005	−8.728	1.44	0.11
	Ni–S	4.7 ± 0.7	0.222 ± 0.001	−4.213	7.40	
	Ni–Ni	0.9 ± 0.3	0.249 ± 0.003	−2.669	2.81	
	Ni–Mo	0.6 ± 0.3	0.275 ± 0.003	0	3.60	
Homemade $NiMo/Al_2O_3$†‡ (Ni/Mo = 0.4 mol mol^{-1})	Ni–O	1.5 ± 0.6	0.203 ± 0.005	−8.728	1.44	0.25
	Ni–S	4.8 ± 0.7	0.220 ± 0.001	−4.213	7.40	
	Ni–Ni	0.4 ± 0.3	0.245 ± 0.004	−2.669	2.81	
	Ni–Mo	0.7 ± 0.3	0.273 ± 0.002	0	3.60	

† E_0 and σ^2 were not fitted. ‡ Koizumi *et al.* (2010).

equation (5) was only 0.34%. Fitting results are summarized in Table 2 in comparison with the values obtained with the homemade $NiMo/Al_2O_3$ catalyst (Ni to Mo molar ratio = 0.4) reported in our previous work (Koizumi *et al.*, 2010). Although $NiMoP/Al_2O_3$ (fresh-g) catalyst had two times higher metal loading than the homemade $NiMo/Al_2O_3$ catalyst, the coordination number and interatomic distance of the Ni–S, Ni–Ni and Ni–Mo coordination shells were identical between these two catalysts, suggesting that the Ni–Mo–S phase as well as small Ni_3S_2 species was formed on the fresh-g catalyst. The difference between these two catalysts was the presence or absence of the Ni–O coordination shell, which might be related to different preparation methods of the fresh and homemade catalysts.

The distribution of Ni in the fresh catalyst was also evaluated by pattern-fitting analysis of the *in situ* Ni *K*-edge XANES spectrum. The *in situ* Ni *K*-edge XANES spectrum of the homemade $NiMo/Al_2O_3$ catalyst (Ni to Mo molar ratio = 0.2) was used as the spectrum of the Ni–Mo–S phase, because only the Ni–Mo–S phase was observed in the *in situ* Ni *K*-edge EXAFS spectrum of this catalyst (Koizumi *et al.*, 2010). Pattern-fitting analysis showed that the spectrum of the fresh-g catalyst was fitted with the spectra of the Ni–Mo–S phase and polycrystalline Ni_3S_2 (Fig. 7*a*). Approximately 80% of the total Ni atoms were involved in the formation of the Ni–Mo–S phase (Table 3). These results are of great importance because the number of edge and corner sites of the MoS_2-like slabs estimated from quasi *in situ* TEM and *ex situ* XRD measurements was 104% of the total number of Ni atoms. It was suggested that all the edge and corner sites of the MoS_2-like slabs could not be occupied by Ni atoms.

3.3.2. Spent catalyst. Fig. 5(*b*) displays the Ni *K*-edge $k^3\chi(k)$ spectrum of the spent catalyst measured under high-pressure H_2 atmosphere (approximately 1.0 MPa) after rinsing with toluene in a glove box filled with N_2. In the lower *k* range (≤ 90 nm^{-1}) this spectrum showed similar EXAFS oscillation to the fresh-g catalyst. However, the EXAFS oscillation rapidly attenuated in the higher *k* range. The FT of this Ni *K*-edge $k^3\chi(k)$ spectrum was performed between 39.0 (k_{min}) and 142 nm^{-1} (k_{max}). The thus obtained FT-EXAFS spectrum is shown in Fig. 5(*d*). The major difference between the spent and fresh-g catalysts was that only a broad peak was observed at around 0.18 nm (not phase-shift corrected) in the spectrum of the spent catalyst. The weak peak related to the formation of the Ni–Mo–S phase was not clearly observed in this spectrum. Instead, a shoulder peak was visible at around 0.20 nm (not phase-shift corrected) in the spectrum of the spent catalyst, suggesting that the intense Ni–Ni peak related

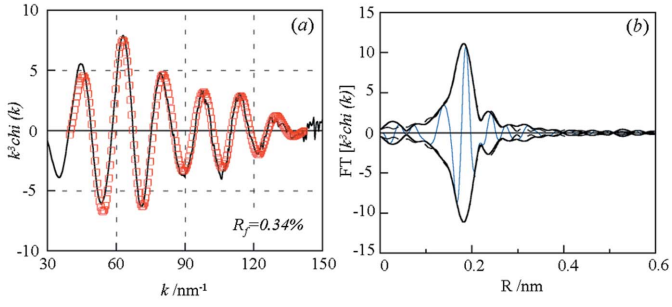

Figure 6
Best-fitting results for the fresh-g catalyst. Fitted data are represented by squares. The R_f value defined by equation (5) is also included in the figures.

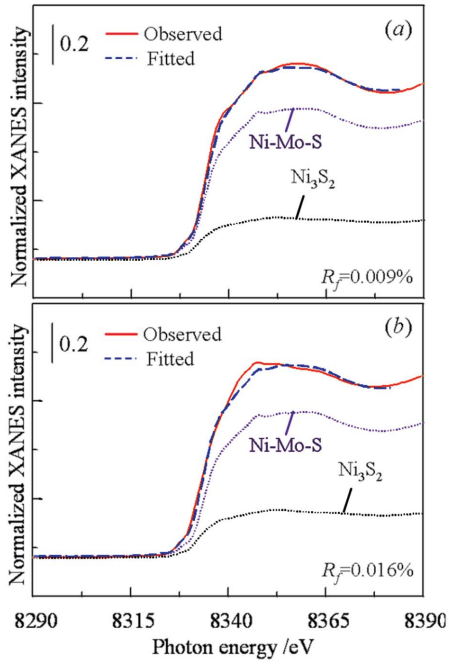

Figure 7
Ni *K*-edge XANES spectra of (*a*) fresh-g and (*b*) spent catalysts. Broken lines represent fitted data. The R_f value defined by equation (6) is also included in the figures. Fitting with XANES spectra of Ni_3S_2 powder and Ni–Mo–S phase.

Table 3
Ni repartitions over fresh-g and spent catalyst evaluated by pattern-fitting analysis of the *in situ* Ni *K*-edge XANES spectrum.

Catalyst	Ni–Mo–S phase	Ni_3S_2 species
Fresh-g	78%	22%
Spent	75%	25%

to the Ni_3S_2 species overlapped the Ni–Mo peak of the Ni–Mo–S phase.

In contrast with the fresh catalyst, curve-fitting analysis showed that the Ni–O coordination shell was necessary to obtain a satisfactory fitting quality for the spent catalyst. This suggested that some of the Ni species in the spent catalyst was oxidized, probably during sampling of the spent catalysts. Curve-fitting analysis was thus performed using the Ni–O, Ni–S, Ni–Ni and Ni–Mo coordination shells. To make the number of parameters comparable with N_{idp}, the inner potential and Debye–Waller factor of each coordination shell were fixed at the values obtained from the polycrystalline NiO, Ni_3S_2 and Ni foil. Best-fitting results are shown in Figs. 8(*a*) and 8(*b*). Optimized structural parameters are summarized in Table 2. From this table it is seen that the Ni–Ni coordination number was approximately three times greater than the value obtained with the fresh-g catalyst. This indicated that the Ni_3S_2 species was sintered during ultra-deep HDS of gas oil, as suggested by *ex situ* XRD and quasi *in situ* TEM/EDX measurements. On the other hand, the Ni–Mo coordination numbers for the fresh-g and spent catalysts were identical within error of the EXAFS measurement. It is also to be noted that, when the fitting was conducted using the Ni–C coordination shell instead of Ni–O coordination shell, the fitting quality was significantly lowered, showing negligible contribution of Ni carbide-like species in the Ni *K*-edge EXAFS spectrum of the spent catalyst.

Pattern-fitting analysis of the quasi *in situ* Ni *K*-edge XANES spectrum of the spent catalyst was performed using the spectra of Ni–Mo–S and polycrystalline Ni_3S_2 (Fig. 7*b*). 75% of the total Ni atoms were still involved in the formation of the Ni–Mo–S phase (Table 3), showing that the Ni–Mo–S phase is preserved on the spent catalyst.

4. Discussion

4.1. Structural changes of Ni species during ultra-deep HDS of gas oil

Eijsbouts *et al.* (2005) recently investigated the surface structure of spent NiMo catalysts from ultra-deep HDS of light gas oil in a trickle bed reactor at 613 K and 4.5 MPa for five days. After extraction of residual gas oil from the spent catalysts with toluene, in some cases, followed by evacuation at 423 K, Ni_3S_2 agglomerates (5–50 nm size) were observed by *ex situ* TEM/EDX measurement of these spent catalysts. On the other hand, MoS_2 dispersion calculated from TEM micrographs was still high. Therefore, they suggested that Ni atoms were segregated from the Ni–Mo–S phase during ultra-deep HDS of gas oil. Similarly, Co sulfide agglomerates were

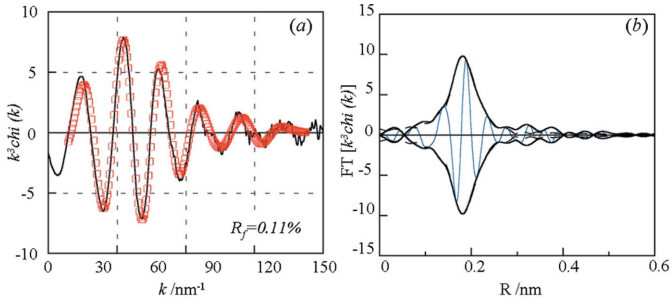

Figure 8
Best-fitting results for the spent catalyst. Fitted data are represented by squares. The R_f value defined by equation (5) is also included in the figures.

observed by *ex situ* TEM/EDX measurement on spent CoMo catalysts from ultra-deep HDS of gas oil in commercial HDS units for two years (Eijsbouts *et al.*, 2007), whereas metallic Co phase was detected by *ex situ* X-ray scattering measurement using a synchrotron radiation source when the catalyst was subjected to HDS of SRGO in a commercial plant for four years (de la Rosa *et al.*, 2004).

In this work the agglomerations of Ni_3S_2 crystallites were observed by *ex situ* XRD and quasi *in situ* TEM/EDX measurement of the spent NiMo catalyst from ultra-deep HDS of gas oil in the commercial HDS unit for two years. Such agglomerates were never observed in the fresh-g catalyst sulfided under high-pressure conditions. *Ex situ* XRD and quasi *in situ* TEM measurement suggested that the MoS_2-like slabs were slightly sintered during ultra-deep HDS of gas oil, but this sintering was not so serious. The number of edge and corner sites of the MoS_2-like slabs in the spent catalyst was still 90% of the total Ni atoms on the spent catalyst. These results are qualitatively consistent with the previous studies (Eijsbouts *et al.*, 2005, 2007). However, quasi *in situ* Ni *K*-edge XAFS measurement of the spent catalyst showed that the Ni–Mo–S phase was preserved on the spent catalyst. Concerning this discrepancy, it is worth noting that the Ni_3S_2 species was formed as well on the fresh-g catalyst after sulfided pretreatment under high-pressure conditions. Because the Tamman temperature (530 K) of Ni_3S_2 is lower than the reaction temperature, it is reasonable to suggest that the agglomerations of Ni_3S_2 crystallites observed in the spent catalyst are formed by sintering of small Ni_3S_2 species originally present on the fresh catalyst, which reasonably explains the observed phenomena in previous and the present studies. In other words, our results suggested that the deactivation of the NiMo catalyst is not accompanied by segregation of Ni from the Ni–Mo–S phase.

Because the Ni–Mo coordination number of the fresh and spent catalysts was smaller than the ones reported by Louwers & Prins (1992) (0.8–1.5), one might think that the present catalyst has lower dispersion of the Ni–Mo–S phase. Owing to its higher metal loading, the present catalyst might indeed have a lower Ni–Mo–S phase dispersion. However, it should be stressed here that the Ni *K*-edge EXAFS measurement was performed at liquid-N_2 temperature in the study by Louwers & Prins (ambient temperature for EXAFS measurement in

this work). Because of the relatively larger thermal disorder at ambient temperature, curve-fitting analysis tends to provide smaller coordination numbers for the EXAFS spectra measured at ambient temperature. It is also worth noting that a Fourier transform of the Ni *K*-edge $k^3\chi(k)$ spectra was performed over limited k ranges (110–120 nm^{-1}) in the EXAFS analysis by Louwers & Prins. This might lead to unreliable coordination numbers as mentioned in our previous paper (Koizumi *et al.*, 2010). To obtain straightforward results of the dispersion of the Ni–Mo–S phase, further studies are necessary with more sophisticated experimental methods.

4.2. Structural changes of Mo species during ultra-deep HDS of gas oil

Quasi *in situ* TEM measurement in this work showed that the MoS_2-like slabs slightly sintered and destacked during ultra-deep HDS of gas oil. The monolayer slab accounted for 40% of the total MoS_2-like slabs in the spent catalyst which was four times greater than that in the fresh-g catalyst. A similar phenomenon was reported for the spent $CoMo/Al_2O_3$ catalyst from HDS of SRGO in the commercial unit based on *ex situ* X-ray scattering measurement (de la Rosa *et al.*, 2004). The average slab length of the MoS_2-like slabs with each stacking number was then calculated to obtain deeper insight into the morphological change of the MoS_2-like slabs. Results are summarized in Table 4. The monolayer slab in the spent catalyst had a larger size compared with those in the fresh-g and fresh-liq catalysts, whereas the multilayer slabs on these catalysts had similar sizes. This suggests that destacking of the MoS_2-like slabs is accompanied by sintering. On the other hand, quasi *in situ* Ni *K*-edge XAFS measurement showed that the Ni–Mo–S phase is preserved on the spent catalyst, as described above, suggesting that a large amount of the multilayer Ni–Mo–S phase was converted into the monolayer phase during ultra-deep HDS of gas oil. From these results it is reasonable to suggest that the conversion of the multilayer Ni–Mo–S phase into the monolayer phase causes catalyst deactivation during ultra-deep HDS of gas oil. In the previous studies the multilayer MoS_2-like slabs (Daage & Chianelli, 1994) and/or Co(Ni)–Mo–S phase (Fujikawa *et al.*, 2005, 2006; Bouwens *et al.*, 1994; Candia *et al.*, 1984) is thought to show higher HDS activity than the monolayer slabs. Our results are consistent with these previous studies.

In our previous studies (Koizumi *et al.*, 2005*a*,*b*, 2006), HDS activity of the spent catalysts linearly decreased with increasing amount of the carbonaceous compound with graphite-like structure. In this relation, the following point should be made. Guichard *et al.* (2008) showed that coke precursors (such as anthracene) adsorbed on the edges of the Ni–Mo–S phase by density functional theory calculations. Carbon incorporation on the edges of MoS_2 slabs was observed in HDS catalysts as carbide-like entities at the catalyst surface (Chianelli & Berhault, 1999; Berhault *et al.*, 2001, 2002). This carbon in corporation causes the MoS_2 slabs to bend, weakening the stabilization due to van der Waals forces and thus favouring the destacking of the MoS_2 slabs (Berhault *et al.*, 2002). Therefore, the destacking process observed in this study may be related to the deposition of a graphite-like carbonaceous compound.

Table 4
Slab lengths of the MoS_2 clusters calculated for each stacking number of the slabs over the fresh and spent catalysts.

		Stacking number						
Catalyst		1	2	3	4	5	6	7
Fresh-g	Slab length (nm)	4.2	4.0	4.3	4.3	4.8	5.0	–
	Number of slabs	32	177	208	128	45	48	–
Fresh-liq	Slab length (nm)	4.1	3.8	3.5	3.5	4.2	–	–
	Number of slabs	45	123	96	76	10	–	–
Spent	Slab length (nm)	5.4	4.4	4.4	5.1	4.9	4.2	6.1
	Number of slabs	127	226	120	88	45	24	14

5. Conclusions

Quasi *in situ* Ni *K*-edge EXAFS spectroscopy in combination with a high-pressure EXAFS chamber was used to investigate the coordination structure of Ni species in the NiMo catalyst deactivated during ultra-deep HDS of gas oil to obtain a better understanding of its deactivation mechanism. *Ex situ* XRD and quasi *in situ* TEM/EDX measurement was also performed to investigate the morphological change of Ni and Mo species. On the spent catalyst, approximately 300 nm-sized Ni_3S_2 agglomerates were observed by quasi *in situ* TEM/EDX measurement, whereas such agglomerates were never observed in the fresh catalyst. On the other hand, growth of the MoS_2-like slabs in the lateral direction was negligible during ultra-deep HDS of gas oil. Quasi *in situ* Ni *K*-edge EXAFS measurement of the spent catalyst showed that the coordination structure of Ni in the Ni–Mo–S phase was almost identical to the fresh catalyst sulfided under high-pressure conditions. The deactivation of the NiMo catalyst was not accompanied by segregation of Ni from the Ni–Mo–S phase. Because *in situ* Ni *K*-edge EXAFS showed that small Ni_3S_2 species were also formed in the fresh catalyst after sulfiding pretreatment under high-pressure conditions, it was suggested that large Ni_3S_2 agglomerates observed in the spent catalyst were formed by sintering of small Ni_3S_2 species originally present on the fresh catalyst.

Quasi *in situ* TEM/EDX analysis further suggested that the multilayer Ni–Mo–S phase was destacked to form the monolayer Ni–Mo–S phase during ultra-deep HDS of gas oil. The monolayer Ni–Mo–S phase accounted for 40% of the total Ni–Mo–S phases (or the MoS_2-like slabs) on the spent catalyst. Furthermore, this destacking was accompanied with the sintering of the monolayer Ni–Mo–S phase. Such a morphological change was suggested as being one of the important causes of catalysis deactivation. It is also noted that the Ni–Mo coordination number of the fresh and spent catalysts was relatively low (1.0) compared with the ones reported previously. This might suggest low dispersion of the Ni–Mo–S phase in these catalysts, and the above conclusion might apply

only to the catalyst studies in this work. Further studies are necessary to draw general conclusions concerning the deactivation mechanism during ultra-deep HDS of gas oil.

The EXAFS measurements were conducted at the BL9C and NW10A stations at the PF under the approval of PF-PAC (proposal No. 2003G-297, 2008G180). The EXAFS measurements were performed at BL14B2 at SPring-8 with the approval of JASRI (proposal No. 2009B1835). We gratefully thank the staff of PF and SPring-8 for their technical support and their kind help.

References

Amemiya, M., Korai, Y. & Mochida, I. (2003). *J. Jpn. Petrol. Inst.* **46**, 99–104.
Ankudinov, A. L., Ravel, B., Rehr, J. J. & Conradson, S. D. (1998). *Phys. Rev. B*, **58**, 7565–7576.
Berhault, G., Cota Araiza, L., Duarte Moller, A., Mehta, A. & Chianelli, R. R. (2002). *Catal. Lett.* **78**, 81–90.
Berhault, G., Mehta, A., Pavel, A. C., Yang, J., Rendon, L., Yácaman, M. J., Araiza, L. C., Moller, A. D. & Chianelli, R. R. (2001). *J. Catal.* **198**, 9–19.
Bouwens, S. M. A. M., Vanzon, F. B. M., Vandijk, M. P., Vanderkraan, A. M., Debeer, V. H. J., Candia, R., Sorensen, O., Villadsen, J., Topsøe, N. Y., Clausen, B. S. & Topsøe, H. (1994). *Bull. Soc. Chim. Belg.* **93**, 763–773.
Callejas, M. A., Martínez, M. T., Blasco, T. & Sastre, E. (2001). *Appl. Catal. A*, **218**, 181–188.
Candia, R., Sorensen, O., Villadsen, J., Topsøe, N. Y., Clausen, B. S. & Topsøe, H. (1984). *Bull. Soc. Chim. Belg.* **93**, 763–773.
Chang, C. L., Tao, Y. K., Swinnea, J. S. & Steinfink, H. (1987). *Acta Cryst.* C**43**, 1461–1465.
Chianelli, R. R. & Berhault, G. (1999). *Catal. Today*, **53**, 357–366.
Christensen, S. V., Bartholdy, J., Hansen, P. L., Conner, W. C., Fraissard, J., Bonardet, J. L. & Ferrero, M. (1994). *Stud. Surf. Sci. Catal.* **87**, 165–172.
Daage, M. & Chianelli, R. R. (1994). *J. Catal.* **149**, 414–427.
Díez, F., Gates, B. C., Miller, J. T., Sajkowski, D. J. & Kukes, S. G. (1990). *Ind. Eng. Chem. Res.* **29**, 1999–2004.
Díez, F., Sajkowski, D. J. & Gates, B. C. (1992). *Fuel Process. Tech.* **31**, 43–53.
Egiebor, N. O., Gray, M. R. & Cyr, N. (1989). *Appl. Catal.* **55**, 81–91.
Eijsbouts, S. & Inoue, Y. (1994). *Stud. Surf. Sci. Catal.* **92**, 429–432.
Eijsbouts, S., van den Oetelaar, L. C. A., Louwen, J. N., van Puijenbroek, R. R. & van Leerdam, G. C. (2007). *Ind. Eng. Chem. Res.* **46**, 3945–3954.
Eijsbouts, S., van den Oetelaar, L. C. A. & van Puijenbroek, R. R. (2005). *J. Catal.* **229**, 352–364.
Fujii, M., Yoneda, T., Satou, M. & Sanada, Y. (2000). *Sekiyu Gakkaishi*, **43**, 149–156.
Fujikawa, T., Kato, M., Ebihara, T., Hagiwara, K., Kubota, T. & Okamoto, Y. (2005). *J. Jpn. Petrol. Inst.* **48**, 114–120.
Fujikawa, T., Kimura, H., Kiriyama, K. & Hagiwara, K. (2006). *Catal. Today*, **111**, 188–193.
Furimsky, E. & Massoth, F. E. (1999). *Catal. Today*, **52**, 381–495.
Gualda, G. & Kasztelan, S. (1994). *Stud. Surf. Sci. Catal.* **88**, 145–154.
Guichard, B., Roy-Auberger, M., Devers, E., Legens, C. & Raybaud, P. (2008). *Catal. Today*, **130**, 97–108.
Guichard, B., Roy-Auberger, M., Devers, E., Pichon, C. & Legens, C. (2009). *Appl. Catal. A*, **367**, 9–22.
Hadjiloizou, G. C., Butt, J. B. & Dranoff, J. S. (1992). *J. Catal.* **135**, 27–44.
Hauser, A., Stanislaus, A., Marafi, A. & Al-Adwani, A. (2005). *Fuel*, **84**, 259–269.
Higashi, H., Takahashi, T. & Kai, T. (2002). *J. Jpn. Petrol. Inst.* **45**, 127–134.
Idei, K., Takahashi, T. & Kai, T. (2002*a*). *J. Jpn. Petrol. Inst.* **45**, 295–304.
Idei, K., Takahashi, T. & Kai, T. (2002*b*). *J. Jpn. Petrol. Inst.* **45**, 305–313.
Idei, K., Takahashi, T. & Kai, T. (2003). *J. Jpn. Petrol. Inst.* **46**, 45–52.
Iijima, M., Mochizuki, T., Koizumi, N. & Yamada, M. (1997). *Sekiyu Gakkaishi*, **40**, 401–407.
Jong, K. P. de, Kuipers, H. P. C. E. & van Veen, J. A. R. (1991). *Stud. Surf. Sci. Catal.* **68**, 289–296.
Jong, K. P. de, Reinalda, D. & Emeis, C. A. (1994). *Stud. Surf. Sci. Catal.* **88**, 155–166.
Koide, R., Fukase, S., Al-Barood, A., Al-Dolama, K., Stanislaus, A. & Absi-Halabi, M. (1999). *Stud. Surf. Sci. Catal.* **122**, 419–422.
Koizumi, N., Hamabe, Y., Jung, S., Suzuki, Y., Yoshida, S. & Yamada, M. (2010). *J. Synchrotron Rad.* **17**, 414–424.
Koizumi, N., Urabe, Y., Hata, K., Shingu, M., Inamura, K., Sugimoto, Y. & Yamada, M. (2005*a*). *J. Jpn. Petrol. Inst.* **48**, 204–215.
Koizumi, N., Urabe, Y., Inamura, K., Itoh, T. & Yamada, M. (2005*b*). *Catal. Today*, **106**, 211–218.
Koizumi, N., Urabe, Y., Suzuki, H., Itoh, T. & Yamada, M. (2006). *Prepr. Am. Chem. Soc. Div. Pet. Chem.* **51**, 333–337.
Kumata, F., Seki, H., Saito, T. & Yoshimoto, M. (2001). *Sekiyu Gakkaishi*, **44**, 252–258.
Liang, K. S., Chianelli, R. R., Chien, F. Z. & Moss, S. C. (1986). *J. Non-Cryst. Solids*, **79**, 251–273.
Louwers, S. P. A. & Prins, R. (1992). *J. Catal.* **133**, 94–111.
Marafi, M. & Stanislaus, A. (1997). *Appl. Catal. A*, **159**, 259–267.
NEDO (2002). *Research and Development of Petroleum Refining Pollutant Reduction*, NEDO Activity Report, p. 82.
Nowack, E., Schwarzenbach, D. & Hahn, Th. (1991). *Acta Cryst.* B**47**, 650–659.
Rooksby, H. P. (1948). *Acta Cryst.* **1**, 226.
Rosa, M. P. de la, Texier, S., Berhault, G., Camacho, A., Yácaman, M. J., Mehta, A., Fuentes, S., Montoya, J. A., Murrieta, F. & Chianelli, R. R. (2004). *J. Catal.* **225**, 288–299.
Roy, M. & Gurman, S. J. (1999). *J. Synchrotron Rad.* **6**, 228–230.
Sahoo, S. K., Ray, S. S. & Singh, I. D. (2004). *Appl. Catal. A*, **278**, 83–91.
Seki, H. & Yoshimoto, M. (2001*a*). *Sekiyu Gakkaishi*, **44**, 102–108.
Seki, H. & Yoshimoto, M. (2001*b*). *Sekiyu Gakkaishi*, **44**, 147–153.
Seki, H. & Yoshimoto, M. (2001*c*). *Sekiyu Gakkaishi*, **44**, 154–162.
Seki, H. & Yoshimoto, M. (2001*d*). *Sekiyu Gakkaishi*, **44**, 259–264.
Stern, E. A. (1993). *Phys. Rev. B*, **48**, 9825–9827.
Swanson, H. E. & Tatge, E. (1953). *Natl. Circ.* **1**, 13.
Ternan, M., Furimsky, E. & Parsons, B. I. (1979). *Fuel Process. Tech.* **2**, 45–55.
Yamazaki, M., Magara, H., Koizumi, N. & Yamada, M. (1999). *Stud. Surf. Sci. Catal.* **126**, 155–162.
Zeuthen, P., Bartholdy, J., Wiwel, P. & Cooper, B. H. (1994). *Stud. Surf. Sci. Catal.* **88**, 199–206.
Zeuthen, P., Cooper, B. H., Clark, F. T. & Arters, D. (1995). *Ind. Eng. Chem. Res.* **34**, 755–762.